# Activation of rod input in a model of retinal degeneration reverses retinal remodeling and induces formation of normal synapses, circuitry and visual signaling in the adult retina

Running title: Visual signaling after retinal remodeling

Tian Wang[1], Johan Pahlberg[2§], Jon Cafaro[3§],
Alapakkam P. Sampath[2*], Greg D. Field[3*], and Jeannie Chen[1*]

Zilkha Neurogenetic Institute, Department of Physiology and Neuroscience, Keck School of Medicine, University of Southern California, Los Angeles, CA 90089
Department of Ophthalmology, Stein Eye Institute, University of California, Los Angeles, CA 90095
Department of Neurobiology, Duke University School of Medicine, Durham, NC, USA

[§]These authors contributed equally to this work

*Correspondence should be addressed to either A.P. Sampath, G. Field or J. Chen.
Email: asampath@jsei.ucla.edu, field@neuro.duke.edu, jeannie@usc.edu

**Acknowledgements:** This work was supported by National Institute of Health grants EY027193 (APS, GDF, and JC); EY12155 and EY027387 (JC); an unrestricted grant from Research to Prevent Blindness to the Department of Ophthalmology, UCLA; and Jules Stein Eye Institute Core Grant EY00331 (APS). We thank Dr. M. Scalabrino for comments on the manuscript, Dr. K.Martemyanov for providing the mGluR6 antibody, Dr. C. Craft for providing the cone arrestin (ARR3) antibody and Dr. S. Ruffins at the USC microscopy core for his help with confocal imaging.

**Conflict of Interest:** The authors declare no competing financial interests.

**Key words**: Neural plasticity, neural transmission, retinal circuitry, retinal degeneration, gene therapy, cGMP-gated channel, photoreceptor cell death.

## Abstract

A major cause of human blindness is the death of rod photoreceptors. As rods degenerate, synaptic structures between rod and rod bipolar cells dissolve and the rod bipolar cells extend their dendrites and occasionally make aberrant contacts. Such changes are broadly observed in blinding disorders caused by photoreceptor cell death and is thought to occur in response to deafferentation. How the remodeled retinal circuit affect visual processing following rod rescue is not known. To address this question, we generated transgenic mice wherein a disrupted cGMP-gated channel (CNG) gene can be repaired at the endogenous locus and at different stages of degeneration by tamoxifen-inducible cre-mediated recombination. In normal rods, light-induced closure of CNG channels leads to hyperpolarization of the cell, reducing neurotransmitter release at the synapse. Similarly, rods lacking CNG channel exhibit a resting membrane potential that was ~10mV hyperpolarized compared to WT rods, indicating diminished glutamate release. Retinas from these mice undergo stereotypic retinal remodeling as a consequence of rod malfunction and degeneration. Upon tamoxifen-induced expression of CNG channels, rods recovered their structure and exhibited normal light responses. Moreover, we show that the adult mouse retina displays a surprising degree of plasticity upon activation of rod input. Wayward bipolar cell dendrites establish contact with rods to support normal synaptic transmission, which is propagated to the retinal ganglion cells. These findings demonstrate remarkable plasticity extending beyond the developmental period and support efforts to repair or replace defective rods in patients blinded by rod degeneration.

## Significance Statement

Current strategies for treatment of neurodegenerative disorders are focused on the repair of the primary affected cell type. However, the defective neuron functions within a complex neural circuitry, which also becomes degraded during disease. It is not known whether a rescued neuron and the remodeled circuit will establish communication to regain normal function. We show that the adult mammalian neural retina exhibits a surprising degree of plasticity following rescue of rod photoreceptors. The wayward rod bipolar cell dendrites re-establish contact with rods to support normal synaptic transmission, which is propagated to the retinal ganglion cells. These findings support efforts to repair or replace defective rods in patients blinded by rod cell loss.

## Introduction

Diseases that afflict sensory systems typically result from deficiencies within the sensory receptor cells themselves, either within sensory transduction or synaptic transmission (Bermingham-McDonogh and Reh, 2011). Deficits in visual processing are no exception, with the majority of blinding diseases resulting from the dysfunction or death of the primary input cells, the retinal rod and cone photoreceptors (Quartilho et al., 2016). Synaptic remodeling of retinal circuits, in particular between photoreceptor cells and their downstream neurons, occur early in retinal degeneration (Soto and Kerschensteiner, 2015). Remodeling of bipolar and horizontal cell dendrites is thought to occur in response to deafferentation (Marc and Jones, 2003). Changes that occur include homeostatic down-regulation of synaptic structures, exuberant extension of dendritic processes which sometimes contact off-target sites (Marc and Jones, 2003; Puthussery and Taylor, 2010), and even switching of post-synaptic receptor types from mGluR to iGluR expression (Chua et al., 2009). In genetically inherited forms of retinal degeneration, synaptic changes may already occur during a critical period of retinal development. It is not known how these changes in retinal circuitry may ultimately limit recovery of normal vision, although several approaches are being implemented to rescue dying photoreceptors using gene therapy, or replace them with stem cells (Scholl et al., 2016; Garg et al., 2017; Yao et al., 2018). To address this gap in knowledge, this study focuses on cellular plasticity in retinal circuits of young adult mice with rod degeneration, and how the synaptic structures and circuits that receive rod input respond to rod rescue.

We genetically engineered a mouse line in which rod function can be uniformly rescued via tamoxifen-induced cre-mediated recombination. The line was generated to lack expression of the cyclic nucleotide gated (CNG) channel beta-1 subunit (CNGB1) due to an insertion of a neomycin cassette at the endogenous gene to disrupt expression (Wang and Chen, 2014; Wang et al., 2017a). This mouse model recapitulates the effects of mutations in human *CNGB1* and *CNGA1* genes that cause autosomal recessive retinitis pigmentosa (Biel and Michalakis, 2007). Without the CNGB1 subunit, the CNG channels in rod outer segments fail to form normally functioning channels, which leads to a slow form of rod death that occurs over 4-6 months (Zhang et al., 2009; Wang et al., 2017a), or longer (Hüttl et al., 2005). Importantly, the neomycin cassette is flanked by loxP sites, which allows for cre-mediated excision and the expression of CNGB1 from the endogenous locus. Thus, this mouse line provides an opportunity to introduce precisely a ‘cure’ for the underlying genetic defect at different time points during degeneration.

We use this novel mouse line to determine the extent to which activating rod input in the degenerating retina allows recovery of the structure and function of well-defined rod-driven retinal circuits in young adult mice. The lack of CNG channels caused stereotypic degenerative changes in the retina that included rhodopsin mislocalization, activation of Müller glia, and a reduction of pre- and post-synaptic proteins between rods and rod bipolar cells by as early as 4 weeks of age. Signal transmission from rods to rod bipolar cells was abrogated and sensitivity of retinal ganglion cells (RGCs) was reduced ~100-fold. Tamoxifen-induced restoration of CNG channel expression initiated at 4 weeks of age led to an expected recovery of rod photoreceptor function. Importantly, we show that initiation of rod input in the deafferented adult retina also induced a high degree of structural plasticity between rods and their primary postsynaptic partner, rod (ON) bipolar cells. Specifically, rod bipolar cell dendrites sprouted fine tips and mGluR6 clusters formed on these tips which made new synapses with rods. This structural transformation resulted in near-normal light responses in both bipolar cells and retinal ganglion cells, the output neurons of the retina. Our findings indicate substantial plasticity in the adult mammalian retina, suggesting favorable outcomes for interventions targeting the rescue of dysfunctional rods from death.

## Materials and Methods

**Generation of transgenic mice.** The use of mice in these experiments was in accordance with the National Institutes of Health guidelines and the Institutional Animal Care and Use Committee of our respective universities. Targeting of the neoloxP to the *Cngb1* locus in mouse embryonic stem cells and generation of transgenic mice from verified stem cell clones were described previously (Chen et al., 2010). The CAGGCre-ER$^{TM}$ transgenic line, Tg(CAG-cre/Esr1*)5Amc/J, was obtained from the Jackson Laboratory and crossed with *Cngb1*$^{neo/neo}$ mice.

**Tamoxifen treatment.** One-hundred mg tamoxifen was dissolved in 500 µl 95% ethanol and diluted with 4.5 ml corn oil to give final concentration of 20 mg/ml. Four-week-old cre-positive were given a dose of 3 mg/25 g body weight by oral gavage for 4 or 7 consecutive days. In control experiments shown in Fig. 1, some cre-negative mice did not receive tamoxifen. For all other experiments, cre-negative littermate mice were also treated with tamoxifen to control for the possible effect of tamoxifen on photoreceptor cell survival (Wang et al., 2017b).

**PCR genotyping.** Genomic DNA was isolated from the neural retina. Three PCR primers were used to detect the presence or absence of the neoloxP cassette. Primer 1 sequence

143 (GTTTTATGTAGCAGAGCAGGGAC) is located on intron 19, primer 2 sequence
144 (GAGGAGTAGAAGGTGGCGC) is on neoloxP, and primer 3 sequence
145 (CCACTCCTTAGTACATACCTAAGC) is located on exon 20. Product size of 620 bp from
146 primer pairs (2+3) indicates the presence of neoloxP, and a 802 bp PCR band from primer pairs
147 (1+3) indicates the absence of the neoloxP insert.
148
149 **Retinal morphology.** Mice were rendered unconscious by isofluorane inhalation and
150 immediately followed by cervical dislocation. Retinal sections were prepared as previously
151 described (Concepcion and Chen, 2010; Wang and Chen, 2014). Briefly, before enucleation,
152 eyes were marked for orientation by cauterization on the superior aspect of the cornea. Eyes
153 were placed in ½ Karnovsky buffer (2.5% glutaraldehyde, 2% formaldehyde in 0.1 M cacodylate
154 buffer, pH 7.2). The cornea and lens were removed, and the remaining eyecup was further fixed
155 overnight. Fixed eyes were rinsed in 0.1 M cacodylate buffer, fixed for 1 h in 1% $OsO_4$,
156 dehydrated in graded EtOH and embedded in epoxy resin. Eyecups were hemi-sected along the
157 superior-inferior axis, and one µm sections along the central meridian were obtained for light
158 micrographs.

159 **Immunocytochemistry.** Eyecups were prepared as described above, except the tissues were
160 dissected in cold 4% formaldehyde in PBS and further fixed for 15 min on ice. For frozen
161 sections, eyecups were rinsed in cold PBS, placed in 30% sucrose for 1 h, embedded in Tissue-
162 Tek® O.C.T. Compound (Sakura® Finetek) and flash frozen in liquid $N_2$. Ten µm frozen
163 sections were obtained. For retinal flat mounts, four relaxing cuts (0°, 90°, 180°, 270°) were
164 made on the edge of the neural retina and the flattened tissue was immobilized on a piece of
165 nitrocellulose membrane (Whatman ®, GE Healthcare Life Sciences), photoreceptor side down,
166 as described (Anastassov et al., 2017). The tissues were incubated with the following
167 antibodies: rhodopsin 1D4 (generously provided by R. Molday), GFAP (AB5804, Millipore),
168 CtBP2 (612044, BD Biosciences), PKC (ab32376, Abcam), mGluR6 (generously provided by K.
169 Martemyanov), ARR3 (generously provided by C. Craft). Images were acquired on a Zeiss
170 LSM800 confocal microscope. For quantifications of mGluR6 puncta, images were imported into
171 Fiji (ImageJ2), adjusted to similar threshold and the number and areas of puncta were quantified
172 using the analyze particles function.

173 **Western blots.** Each isolated retina was homogenized in 150 µl buffer (150mM NaCl, 50mM
174 Tris pH 8.0, 0.1% NP-40, 0.5% deoxycholic acid, 0.1 mM PMSF and complete mini protease
175 inhibitor (Roche Applied Sciences), incubated with DNase I (30U, Roche Applied Sciences) at
176 room temperature for 30 min. An equal amount of retinal homogenate from each sample was
177 electrophoresed on 4-12% Bis-Tris SDS-PAGE Gel (Invitrogen). Protein was transferred onto
178 nitrocellulose membrane (Whatman ®, GE Healthcare Life Sciences) and incubated overnight
179 with the following primary antibodies: rabbit anti-PDE polyclonal antibody (PAB-06800,
180 Cytosignal), rabbit anti-ROS-GC1 polyclonal antibody (sc50512, Santa Cruz), mouse Anti-$G_t\alpha$
181 antibody (371740, EMD4Biosciences), rabbit polyclonal anti-GCAP1 and GCAP2 antibodies
182 (Hoyo et al., 2014; Wang and Chen, 2014), mouse anti-CNGB1 4B1 antibody (Poetsch et al.,
183 2001), mouse anti-CNGα antibody PMc 1D1 (Cook et al., 1989), mouse NCKX1 8H6 antibody
184 (Vinberg et al., 2015) and mouse anti-Actin antibody (MAB1501, Millipore). The membranes
185 were then incubated with fluorescently labeled secondary antibodies (1:10,000, LI-COR
186 biosciences, 926-31081) at room temperature for 1 hour and detected by Odyssey infrared
187 imaging system.

188

189 **Whole retina and single-cell recordings from rods and bipolar cells.** Mice were maintained
190 on a normal 12-hour day-night cycle and were dark-adapted overnight (>12-h) prior to
191 experiments. All further manipulations were performed in total darkness under infrared
192 illumination visualized with infrared image converters (BE Meyers, WA). Following euthanasia,
193 eyes were enucleated, the lens and cornea were removed, and eyecups were stored in
194 darkness at 32°C in Ames' media buffered with sodium bicarbonate (Sigma, Cat# A1420)
195 equilibrated with 5% $CO_2$/ 95% $O_2$.
196 *Trans*-retinal electroretinograms (ERGs) were recorded from isolated retinas as
197 described previously (Pahlberg et al., 2017). Retinas were mounted photoreceptor side-up over
198 a machined hole in a recording chamber. The tissue was superfused in darkness with 35-37°C
199 Ames' media buffered with sodium bicarbonate and equilibrated with 5% $CO_2$/ 95% $O_2$ (pH ~
200 7.4). An additional 10 mM of BaCl was added to the solution facing the inner retina to mitigate
201 Müller cell activity. The *trans*-retinal potential change to flashes of light, delivered from a
202 standard light bench, was measured using Ag/AgCl half-cells connected to a differential
203 amplifier (Model DP-311; Warner Instruments). Recordings were sampled at 1 kHz and low-
204 pass filtered at 30 Hz.
205 Recordings of the photovoltage from individual rods and rod bipolar cells was made by
206 whole-cell patch clamp from dark-adapted retinal slices as described previously (Pahlberg et al.,

207 2017). Briefly, a small piece of dark-adapted retina was embedded in low-gelling temperature
208 agar, slices were cut on a vibrating microtome, transferred into a recording chamber, and
209 superfused with Ames' media equilibrated with 5%$CO_2$/95%$O_2$ while maintained at 35-37°C.
210 The pipette internal solution consisted of (in mM): 125 K-Aspartate, 10 KCl, 10 HEPES, 5 N-
211 methyl glucamine-HEDTA, 0.5 $CaCl_2$, 1 ATP-Mg, 0.2 GTP-Mg; pH was adjusted to 7.2 with N-
212 methyl glucamine hydroxide. Light-evoked responses were recorded following the delivery of 10
213 ms flashes from a blue LED ($\lambda_{max}$ ~ 470 nm, full width half maximum ~ 30 nm) whose strength
214 varied from producing a just-measurable response, and increased by factors of 2. Recordings
215 were sampled at 1 kHz and low-pass filtered at 300 Hz.
216

217 **Retinal ganglion cell recording, stimulation and analysis**

218 Retinal ganglion cells were recorded from dorsal retina using a large scale, dense
219 hexagonal multi-electrode array covering ~0.34mm$^2$ of the retina (MEA, (Field et al., 2010) 519
220 electrodes with 30 μm spacing). The pigmented epithelium remained attached to the retina for
221 these recordings. The retina was perfused with Ames' solution (30-31°C) bubbled with 95/5%
222 $O_2$/$CO_2$. Spikes were identified and assigned to specific RGCs on the MEA as previously
223 described (Yu et al., 2017). Dim flashes were delivered at 3 s intervals using a 490 nm LED.
224 Light intensity was controlled using pulse duration, 2-8 ms, and neutral density filters. Dim flash
225 responses were measured by counting spikes on each trial within a 100 ms window that was
226 centered on the peak of the peristimulus time histogram.

227 **Experimental design and statistical analyses**

228 Because our initial studies did not show gender-specific differences, the genders were
229 pooled. RGC response thresholds were measured from three *Cngb1ΔCaM* retinas (102-232
230 cells), five *Cngb1*$^{neo/neo}$ retinas (100-336 cells) and three *Cngb1*$^{neo/neo}$ rescue retinas (53-186
231 cells). Cumulitive threshold histograms were calculated in each tissue and averaged across all
232 retinas within a condition. A two tailed Kolmogorov-Smirnov goodness-of-fit hypothesis test was
233 used to assess the statistical difference between average cumulative histograms. The fraction
234 of cells for which no response surpassed threshold was also measured in each recorded retina.
235 A two sample t-test was used to evaluate significance between conditions.
236
237
238

## Results

### *Generation of a novel animal model of genetically reversible rod degeneration*

One challenge to identifying how plasticity among inner retinal neurons impacts functional recovery is the lack of an experimental system that is non-invasive and allows for stringent regulation of the timing and uniformity of rescue. For example, viral-mediated (gene therapy) approaches for treating rod dysfunction and death (1) take weeks for expression to occur; (2) they do not infect all targeted cells; (3) they may not drive proper protein expression levels; (4) and the subretinal injections used for viral delivery can damage the retina. A systematic investigation into the consequences of rod degeneration and subsequent rescue of the retinal circuitry requires an experimental system wherein both events occur uniformly in the retina. Towards this goal, a neoloxP cassette was inserted into intron 19 of the *Cngb1* gene by homologous recombination in mouse embryonic stem cells (Fig. 1A). Mice harboring this insertion were subsequently derived (*Cngb1*$^{neo/neo}$). The presence of the cassette disrupted a splice site and prevented CNGB1 expression (Fig. 1B). Expression of CNGA1 was also substantially attenuated (Fig. 1B), a phenomenon attributed to mis-trafficking (Hüttl et al., 2005) and structural stability conferred by association of both subunits. The expression levels of other major phototransduction proteins were minimally perturbed in retinas of 1-month old (1 MO) mice (Fig. 1B, NCKX1, GC1, PDE6A, and GNAT1). Consistent with previous reports on conventional *Cngb1* knockout mice (Hüttl et al., 2005; Zhang et al., 2009), the lack of CNG channel expression led to a progressive thinning of the outer nuclear layer over the course of 6 months (Fig. 1C). At two-weeks, the outer nuclear layer (ONL) containing primarily rod photoreceptor cell nuclei reached its maximum thickness. This thickness was reduced by ~20% in 1 MO mice and to ~50% in 2 MO mice. By 6 MO, the ONL was absent. Thus, these mice exhibit slow rod degeneration relative to other commonly used models of rod degenerative diseases, such as *rd1* (Farber and Lolley, 1974) and *rd10* mice (Chang et al., 2007).

As expected, the absence of the CNGB1 recapitulated the stereotypic sequence of events associated with rod degeneration (Marc and Jones, 2003; Puthussery and Taylor, 2010; Soto and Kerschensteiner, 2015). For example, rhodopsin mislocalization and activation of Müller glia were observed in 4-week old *Cngb1*$^{neo/neo}$ mice (Fig. 1, compare F, G with control retina, D and E).

We also observed in *Cngb1*$^{neo/neo}$ mice that synaptic contacts between rods and rod bipolar cells were structurally abnormal. Immunohistochemistry using a marker for the presynaptic ribbon protein CtBP2 (ribeye) and the post-synaptic glutamate receptor, mGluR6,

273 revealed clear differences between *Cngb1*$^{neo/neo}$ and control retinas. In control retinas, these
274 structures were closely apposed, and both were contained within a well-defined outer plexiform
275 layer (Fig. 1H, OPL). However, in *Cngb1*$^{neo/neo}$ retinas these structures were more dispersed,
276 with synaptic ribbons retracted from rod spherules and some were situated deep into the
277 photoreceptor nuclear layer (ONL, Fig. 1I, arrows). The ultrastructure of rod synapses was
278 further evaluated by transmission electron microscopy (TEM, Fig. 1J and K). A normal rod
279 spherule (blue) contains a single large mitochondria (yellow) and encompasses a synaptic triad
280 consisting of a single ribbon (red) along with horizontal (orange) and rod bipolar cell (green)
281 processes. The majority of imaged rod spherules from control retinas exhibited this structure.
282 Dyads were also frequently observed when one or another component was out of the plane of
283 the TEM section. Of the 27 fields taken from 4 control C57 retinas, 122 synapses were counted
284 (4.5 synapses per field) wherein 64% were triads and 36% were dyads. However, in 1 MO
285 *Cngb1*$^{neo/neo}$ retinas, the frequency of observing synapses and triadic structures were both
286 reduced (Fig. 1K). Of 31 TEM fields taken from 4 *Cngb1*$^{neo/neo}$ retinas, 64 synapses were
287 counted (2.1 synapses per field) wherein only 22% were triads and 78% of were dyads. Note, at
288 1 MO, only 20% of rods had died, yet there was >50% reduction in contacts between rods and
289 rod bipolar cells. Furthermore the contacts that persisted were largely abnormal in structure.
290 These results demonstrate that *Cngb1*$^{neo/neo}$ mice exhibit stereotypic slow rod degeneration and
291 that synaptic structures between rods and rod bipolar cells were disrupted.
292
293 **Lack of CNGB1 expression attenuated rod photoresponses and eliminated rod bipolar**
294 **cell light responses.**
295 Previous work has indicated that lack of CNGB1 expression compromises rod vision
296 (Biel and Michalakis, 2007). To verify compromised rod function in *Cngb1*$^{neo/neo}$ mice, we
297 performed *ex vivo* whole-retina electroretinograms (ERG) under scotopic conditions. The ERG
298 reflects the averaged activity across all retinal neurons (Granit, 1933). ERGs from C57 retinas
299 exhibited a well characterized biphasic response (Fig 2A; see also (Saszik et al., 2002)) with the
300 initial negative-voltage deflection (a-wave) indicative of the rod hyperpolarization to the flash
301 stimulus, and the subsequent positive-voltage rebound indicative of predominantly the rod
302 bipolar cell depolarization. Recordings were also performed on control *Cngb1*Δ*CaM* mice in
303 which the calmodulin binding site was removed (Chen et al., 2010). No differences were
304 observed between *Cngb1*Δ*CaM* and C57 retinas (data not shown).
305 ERGs from 1 MO *Cngb1*$^{neo/neo}$ retinas exhibit a diminished scotopic a-wave with reduced
306 sensitivity (Fig. 2B), indicating minimal rod signaling without CNGB1 expression. The light

307 response is not fully eliminated in these rods; this is likely due to residual activation of
308 homomeric channels composed of CNGA1 (see Discussion). Furthermore, ERGs from
309 *Cngb1*$^{neo/neo}$ retinas did not exhibit a b-wave under scotopic conditions, indicating a lack of
310 measurable rod-to-rod bipolar signal transmission at this gross level. This observation
311 complements the abnormal synaptic structures observed between rods and rod bipolar cells via
312 light and electron microscopy. Together, these results indicate that synaptic transmission
313 between rods and rod bipolar cells is severely dysfunctional in *Cngb1*$^{neo/neo}$ mice. Thus, we
314 sought to determine the extent to which normal synaptic structures and transmission between
315 rods and rod bipolar cells could be recovered by the rescue of CNGB1 expression in mature
316 retinas.
317
318 ***Cre-mediated excision of the NeoLoxP cassette leads to normal CNGB1 expression.***
319 To activate CNGB1 expression in the the *Cngb1*$^{neo/neo}$ retina, we utilized the CAGGCre-
320 ER$^{TM}$ transgene (Hayashi and McMahon, 2002) to enable tamoxifen-dependent, cre-mediated
321 excision of the NeoloxP cassette. We previously demonstrated that mice derived from germline
322 excision of this cassette exhibit normal retinal morphology with a uniform and normal expression
323 level of CNGB1 (Chen et al., 2010). The homologous recombination strategy that introduced
324 the NeoloxP cassette also removed a stretch of 14 amino acids that encompassed the
325 calmodulin binding domain on CNGB1 (Grunwald et al., 1998). Importantly, rods that expressed
326 CNGB1ΔCaM exhibited normal light responses as mentioned above (see also (Chen et al.,
327 2010)). We hypothesize that utilizing the CAGGCre-ER$^{TM}$ transgene would provide temporal
328 control over expression of the functional CNG channel. To determine the efficacy of cre-
329 mediated excision of the neoloxP cassette, four-week-old cre-positive and cre-negative
330 *Cngb1*$^{neo/neo}$ littermate mice were divided into two groups. One group was given tamoxifen for
331 four-consecutive days by oral gavage, and the other group did not receive drug treatment.
332 A PCR strategy was designed to detect the extent of neoloxP excision in genomic DNA
333 extracted from isolated retinas: the primer pair (2+3) detects the presence of the neoloxP insert,
334 whereas primer pair (1+3) gives rise to a diagnostic band when the large neoloxP insert is
335 excised (Fig. 3A). After four-consecutive days of tamoxifen treatment, both sets of primers
336 produced positive bands. This result indicates a mixed population of cells at this stage, some of
337 which have undergone excision while others have not. However, when tamoxifen treatment was
338 given for seven-consecutive days a positive signal was detected only by primers (1+3). This
339 result indicates that following a 7-day tamoxifen treatment, most, if not all cells have undergone

340 neoloxP excision (Fig. 3A, bottom panels). Thus a 7-day treatment was used for further
341 structural and functional studies.
342 To assess the level of protein expression at 6- or 8-weeks (corresponding to 1 or 3
343 weeks after drug treatment), Western blots were prepared from whole retinal homogenates from
344 both cohorts (Fig. 3B). Expression of CNGB1 protein was observed only in tamoxifen-treated,
345 cre-positive mice. No expression was observed in cre-positive mice without drug treatment,
346 indicating a lack of basal recombinase activity. We next examined how excision of the neoloxP
347 insert affected the expression of CNGB1 and other major phototransduction proteins. We found
348 that following neoloxP excision, there was a striking increase in CNGB1 expression (Fig. 3C).
349 There was also an increase in the detected levels of other phototransduction proteins GC1,
350 PDE6A, GNAT1, and GCAP2 (Fig 3C). To determine if this is due to rod rescue, cre-negative
351 and cre-positive *Cngb1*$^{neo/neo}$ littermate mice were administered tamoxifen for 7 consecutive
352 days beginning at 4-weeks, and retinal sections were prepared from 3 MO mice (Fig. 3D and
353 3E). The ONL thickness was greater in cre-positive mice when compare to that from the cre-
354 negative sibling mice, and the rod outer segment structure was organized and of normal length.
355 Expression of CNGB1 exhibited a long term rescuing effect on rod survival (Fig. 3F and 3G,
356 tamoxifen was administered for 4 consecutive days starting at P28), consistent with a previous
357 report on AAV-mediated *Cngb1* gene replacement therapy (Koch et al., 2012). In sum, these
358 data show that the *Cngb1*$^{neo/neo}$ mice allowed us to regulate the expression of CNGB1 from the
359 endogenous locus in a temporally-controlled manner. Further, this excision is nearly complete
360 with a 7-day tamoxifen treatment and that upon expression of CNGB1, the rods exhibit normal
361 morphology and are stably rescued from cell death.
362 We measured the responsiveness of rod photoreceptors following drug treatment in
363 patch-clamp recordings from individual rods in retinal slices. In voltage-clamp ($V_m$ = -40 mV),
364 rods from 1 MO *Cngb1*$^{neo/neo}$ mice displayed diminished response amplitudes (~6-fold) and a
365 ~10-fold reduction in light sensitivity (Fig. 4A), a result consistent with the diminished a-wave in
366 *ex vivo* ERG recordings (Fig. 2B). In current-clamp ($i$ = 0), *Cngb1*$^{neo/neo}$ rods exhibit a resting
367 membrane potential that was ~10 mV hyperpolarized compared to WT rods (-47 ± 1.3 mV (5)
368 vs. -37 ± 2.3 mV (6), mean ± SEM). These results are consistent with reduced CNG channel
369 expression (see Discussion) and indicate reduced glutamate release in darkness. However,
370 rods from tamoxifen treated *Cngb1*$^{neo/neo}$ mice displayed responses with characteristics very
371 similar to C57 mice (Fig. 4B), consistent with near-normal function and rescue of the
372 photoreceptor layer (Fig. 3).
373

374 ***Expression of CNGB1 induces normal synaptic structures between rods and rod bipolar***
375 ***cells.***
376 Given that tamoxifen administration in *Cngb1*$^{neo/neo}$ mice rescued rods from death (Fig.
377 3E) and rescued normal rod light responses (Fig. 4), we next examined the synaptic contacts
378 between rods and rod bipolar cells to determine how rod rescue impacts these structures.
379 Tamoxifen treatment was initiated at 4-weeks for 7 consecutive days, and retinal structure was
380 examined at 3M. Comparisons were made between 1 MO C57 and *Cngb1*$^{neo/neo}$ mice and 3 MO
381 tamoxifen-treated mice to examine the effect of rod rescue that was initiated at 1M. Synaptic
382 structures were labeled in retinal flat mounts stained for the presynaptic ribbon synapse protein
383 (CtBP2, blue) and postsynaptic mGluR6 (orange, Fig. 5A, 5D and 5G). To distinguish between
384 rod and cone synapses, cone pedicles were further labeled with the cone arrestin antibody
385 (ARR3, green). Rod bipolar cell morphology, visualized by PKC$\alpha$ staining, and the mGluR6
386 puncta that decorate their dendritic tips are shown in retinal cross sections (Fig. 5B, 5E and 5H).
387 Control retinas (C57), exhibited a close juxtaposition between the rod's single ribbon and
388 the mGluR6 puncta on the dendritic tips of rod bipolar cells (Fig. 5A and 5B; Fig. 1G). However,
389 in *Cngb1*$^{neo/neo}$ retinas from 1 MO mice, both the number of synaptic ribbons and mGluR6
390 puncta were reduced (Fig. 5D). Rod bipolar cell dendrites were also unevenly distributed in
391 *Cngb1*$^{neo/neo}$ retinas, and the size of the mGluR6 puncta appeared smaller and less uniform in
392 shape (Fig. 5E and Fig. 1H). In contrast, retinas from the tamoxifen-treated, cre-positive
393 littermates exhibited robust staining of synaptic ribbons along with their associated mGluR6
394 puncta (Fig. 5G). Furthermore, rod bipolar cell dendrites were evenly extended and the
395 mGluR6 puncta were larger in size and appeared more uniform in shape (Fig. 5H). To quantify
396 these changes, the number and size of mGluR6 puncta were measured (Fig. 5C, 5F and 5I).
397 For the C57 retina, mGluR6 puncta size of 20- to 30-unit area were the most numerous,
398 whereas in *Cngb1*$^{neo/neo}$ retinas smaller size puncta were more frequent (compare Fig. 5C and
399 5F). The distribution shifted back to larger puncta sizes in the tamoxifen-treated mice (Fig. 5I).
400 These results indicate that inducing expression of CNGB1 in mature retina causes a recovery of
401 synaptic structures between rods and rod bipolar cells.
402
403 ***Rescue of CNGB1 expression in mature retina recovers rod bipolar light responses.***
404 The results above indicate a structural recovery of synapses following expression of
405 CNGB1. In addition to this structural recovery, *ex vivo* whole-retina ERGs revealed a recovery
406 of the rod bipolar cell-driven b-wave with amplitudes similar to control retinas (Fig. 6A). Thus,
407 structural and functional measures broadly indicate recovery of synaptic function between rods

408 and rod bipolar cells. To examine further synaptic function before and following rod rescue, we
409 performed patch clamp recordings from rod bipolar cells in retinal slices. In untreated
410 *Cngb1*$^{neo/neo}$ mice there was a complete absence of functional transmission of between rods and
411 rod bipolar cells (Fig. 6C); 1 MO *Cngb1*$^{neo/neo}$ rod bipolar cells never yielded light-evoked
412 responses (n=15 from 5 retinas), a result consistent with a lack of b-wave in *ex vivo* ERG
413 recordings which represent mass-action of largely rod bipolar cells (Fig. 2B). However, in
414 *Cngb1*$^{neo/neo}$ mice administered tamoxifen for 7 days at 4 weeks of age and recorded at 3 MO,
415 rod bipolar cells exhibited robust light-evoked responses similar to control animals (Fig. 6D).
416 The extent of functional recovery in rod bipolar cells was characterized in plots of the response
417 amplitude versus the flash strength. These intensity-response relationships were fit with a Hill
418 curve and compared quantitatively to control responses. The half-maximal flash strength ($I_{1/2}$)
419 increased by ~2-fold in rescued animals (Fig. 6E), consistent with some rod loss (see
420 Discussion). However, other features of the rod bipolar light response that are critical for
421 function near visual threshold had recovered to near control values. For example, the Hill
422 exponent for the fit of the response-intensity relationship matched that in control, indicating a
423 similar nonlinear relationship between the flash strength and the response amplitude. The
424 extent of nonlinearity reflects the rate of glutamate release from rod synapses (Sampath and
425 Rieke, 2004). In addition, the time course of rod bipolar cell responses was similar in rescued
426 animals (Fig. 6A, 6C, 6E – dashed line), further indicating the anatomical and physiological
427 recovery of synaptic transmission in tamoxifen-treated animals. These results indicate that
428 rescuing rod function in the mature mouse retina produces a cascade of structural and
429 functional recovery in synaptic transmission between rods and rod bipolar cells, and thus the
430 primary rod pathway (Dacheux and Raviola, 1986).
431
432 **Rescuing rods recovers absolute sensitivity of retinal output**
433 Retinal ganglion cells (RGCs) provide the sole output from the retina and can integrate
434 input from thousands of rods, making them the most light-sensitive cells in the retina
435 (Chichilnisky and Rieke, 2005; Field and Sampath, 2017). RGC sensitivity relies on functioning
436 photoreceptors and highly tuned synaptic connections via the primary rod pathway (Field and
437 Rieke, 2002; Sampath and Rieke, 2004). To understand how rescuing rod function in the 1 MO
438 *Cngb1*$^{neo/neo}$ retina impacts RGC sensitivity, we used a large-scale multi-electrode array (MEA)
439 to record spikes from hundreds of RGCs. We tested the sensitivity of the RGCs by stimulating
440 the retina with brief, dim flashes (0.001-10 Rh*/rod) and compared RGC responses in 3 MO
441 control *Cngb1*Δ*CaM*, *Cngb1*$^{neo/neo}$, and 4-5 MO *Cngb1* tamoxifen rescued mice. Flashes

442 producing less than 1 isomerization per rod faithfully produced spike rate modulations in many
443 RGCs from control mice (Fig 7A shows an example cell). The same flash intensities did not
444 reliably modulate the spike output of most RGCs in retinas from 3 MO old *Cngb1*$^{neo/neo}$ mice (Fig
445 7B shows an example cell). Indeed, most RGCs from *Cngb1*$^{neo/neo}$ mice did not show reliable
446 responses until flash intensities exceeded 1 Rh*/rod (Fig 7B$_3$). However, similar to the control
447 retinas, RGC responses were often evident at low flash intensities in 4-5 MO *Cngb1* rescued
448 mice (Fig 7C shows an example cell). These example cells suggest that rod and circuit
449 functionality are broadly and stably rescued in some RGCs for *Cngb1* rescued mice.
450 To measure the extent that sensitivity across the RGC population recovered in *Cngb1*
451 rescued mice, we quantified the response-threshold for all RGCs (N=1954) in MEA recordings
452 from 11 mice (3 control *Cngb1ΔCaM* mice, 3 *Cngb1*$^{neo/neo}$ mice, 5 tamoxifen-treated *Cngb1*
453 mice). RGC response thresholds were quantified as the lowest flash intensity needed to drive
454 the average spike rate change two standard deviations above baseline (eg. Fig 7A$_3$, 7B$_3$, 7C$_3$;
455 see Methods). Average RGC response threshold distributions were similar between control and
456 *Cngb1* rescued mice, but were significantly higher in untreated *Cngb1*$^{neo/neo}$ mice (Fig 7D; KS
457 test, $p<0.05$). Additionally, the fraction of RGCs for which no-threshold response could be
458 measured was similar between control and *Cngb1* rescued mice but significantly higher in
459 untreated *Cngb1*$^{neo/neo}$ mice (Fig 7E; *t*-test, $p<0.05$). These results indicate a broad and lasting
460 recovery of rod and circuit functions in *Cngb1* rescued mice.
461
462 **Discussion**
463
464 In contrast to other neurons, rods and cones are depolarized in darkness and tonically
465 release glutamate through ribbon synapses (Molday and Moritz, 2015), leading to saturation of
466 rod-to-rod bipolar cell synapses (Sampath and Rieke, 2004). Light exposure causes graded
467 hyperpolarization of the photoreceptor cell and suppression of glutamate release. Reductions in
468 glutamate release from photoreceptors that occur during the early process of retinal
469 degeneration lead to homeostatic changes in the downstream neurons and degrade the retinal
470 circuit. This is seen in the dissolution of synaptic structures, dendritic sprouting, formation of
471 ectopic contacts, and gliosis (Marc et al., 2003; Puthussery and Taylor, 2010). Although
472 strategies to rescue and restore function in defective photoreceptors have shown success for
473 regaining some visual function, gene and stem cell therapies for visual restoration are often
474 implemented in the adult; how well these rescued neurons reinstate their detailed circuitries in
475 the remodeled retina is not known. Here we examined functional restoration at the level of inner

476 retinal cells and defined rod-driven circuits in the young adult mouse retina. We show that
477 repairing a primary genetic defect in rods not only restored rod function, but also recovered
478 normal synaptic connectivity with remodeled second order rod bipolar cells.
479
480 **Rod-to-rod bipolar cell synaptic contacts are reduced in *Cngb1$^{neo/neo}$* retina and do not**
481 **support synaptic transmission**
482 The relatively slow photoreceptor degeneration we observe in the *Cngb1$^{neo/neo}$* mouse
483 model, and observed in human patients (Bareil et al., 2001; Biel and Michalakis, 2007), may be
484 due to the fact that it is not a functional null. A small but measurable light response persisted in
485 *Cngb1$^{neo/neo}$* rods from 1 MO mice (Fig. 4B). The residual light response is probably due to the
486 presence of homomeric channels composed of CNGA1 subunits, which are capable of
487 mediating a diminished and desensitized cGMP-dependent current (Kaupp et al., 1989). The
488 small current would reduce $Ca^{2+}$ influx to the outer segment, causing increased levels of cGMP
489 through stimulation of guanylyl cyclases by $Ca^{2+}$-free guanylyl cyclase activating proteins 1 and
490 2 (Mendez et al., 2001; Dizhoor et al., 2010). Elevated cGMP has been shown to be a driver of
491 rod degeneration through activation of protein kinase G (Ma et al., 2015; Wang et al., 2017a).
492 Despite the diminished rod light responses in the *Cngb1$^{neo/neo}$* mice, the utter lack of
493 evidence for light-evoked transmission between rods and rod bipolar cells was unexpected,
494 especially given our ultrastructural evidence showing that the number of triads in the
495 *Cngb1$^{neo/neo}$* rod spherules was reduced, but not fully eliminated (Fig. 1). Therefore, it is
496 surprising that ERGs from *Cngb1$^{neo/neo}$* mice did not exhibit a scotopic b-wave, which is largely
497 contributed by rod bipolar cells (Fig. 2B; (Saszik et al., 2002). This result was further
498 corroborated by patch-clamp measurements from rod bipolar cells that revealed no light
499 response, even for bright flashes delivering ~2000 Rh*/rod (Fig. 6C). We speculate that this
500 defect in synaptic transmission is due to diminished glutamate release at the ribbon synapse
501 given that the lack of CNG channels should act as a source of “equivalent light”, similar to light-
502 induced closure of CNG channels (see also Sampath and Rieke, 2004; Dunn et al., 2006).
503 Supporting this idea, the resting membrane potential of *Cngb1$^{neo/neo}$* rods are ~10 mV
504 hyperpolarized due to their smaller dark current (Fig. 4A). At the rod’s normal resting potential in
505 darkness (~40 mV), calcium enters through the voltage gated channel ($Ca_v1.4$) and supports
506 tonic glutamate release at the ribbon synapse (Waldner et al., 2018). Thus the hyperpolarizing
507 shift in resting potential of *Cngb1$^{neo/neo}$* rods predicts attenuated glutamate release from the rod
508 spherule.

509 Interestingly, suppression of glutamate release at the rod synapse is strongly correlated
510 with synaptic remodeling. Examples include blockade of glutamate release by tetanus toxin
511 (Cao et al., 2015), in knockout mice that lack the presynaptic $Ca_V1.4$ $Ca^{2+}$ channel (Mansergh et
512 al., 2005), and in human patients diagnosed with congenital stationary night blindness (CSNB2)
513 that harbor null mutations in the gene encoding $Ca_V1.4$ (Bech-Hansen et al., 1998; Boycott et
514 al., 2000). Calcium entry through $Ca_V1.4$ channel is required for neurotransmitter release at the
515 ribbon synapse of both rods and cones. The absence of CaBP4 (Haeseleer et al., 2004) or $\alpha2\delta4$
516 (Wang et al., 2017c) that bind and regulate the activity of $Ca_V1.4$, also manifest in retinal
517 remodeling in knockout mice. These plastic changes occurred with minimal photoreceptor cell
518 loss, suggesting that synaptic remodeling is likely driven by suppression of neural transmission,
519 or deafferentation, rather than photoreceptor cell death *per se*. Modest synaptic changes were
520 also observed in RIBEYE knockout retinas. RIBEYE is an essential component of the synaptic
521 ribbon, and its absence abolished all presynaptic ribbons in the retina and severely impaired
522 fast and sustained neurotransmitter release (Maxeiner et al., 2016). Spontaneous miniature
523 release continues to occur without the synaptic ribbon, which may explain the milder retinal
524 remodeling phenotype observed in the RIBEYE knockout retina (Maxeiner et al., 2016).
525 Previous studies on two independent lines of *Cngb1*$^{-/-}$ mice have similarly reported a
526 substantial reduction of light responses from *Cngb1*$^{-/-}$ rods, but in both mouse lines the presence
527 of a rod bipolar cell driven b-wave was observed (Hüttl et al., 2005; Zhang et al., 2009). The
528 reason behind the discrepancy between those and our results is not clear, but may be due to
529 differences in: 1) the degree of rod hyperpolarization caused by the number of functioning
530 homomeric CNGA1 channels and hence the amount of glutamate released by rods in the
531 different mouse lines, 2) the *in vivo* vs. *ex vivo* ERG measurements, or 3) mouse genetic
532 backgrounds.
533
534 **Adult rod bipolar cells demonstrate plastic changes to establish functional contacts with**
535 **rescued rods**
536 The developmental time window for the formation of the rod to rod bipolar cell synapse
537 in mice appears to be from eye opening to postnatal day 30 (P30), during which synaptic
538 proteins are expressed, pre- and post-synaptic molecular complexes form, and the rod bipolar
539 cells develop the appropriate number of dendritic tips that make synaptic contacts with rods
540 (Anastassov et al., 2017). Some of the molecules that guide neurite growth during development
541 are absent at maturity (D'Orazi et al., 2014), and if functional connectivity of the neural retina
542 can only occur during a critical period in development, then one would expect that the adult

543 retina may lack the ability to make such connections when rod activity is switched on after this
544 time window. Such developmental processes would have been disrupted in *Cngb1*$^{neo/neo}$ retinas,
545 wherein pronounced retinal remodeling is evident by P30 (Fig. 1). We show that tamoxifen-
546 induced CNGB1 expression between P28-P34 led to establishment of the rod's circulating
547 current in darkness and normal light responses (Fig. 4). Concomittantly, structural changes
548 were observed at the synapse: rod bipolar cells elaborated fine dendritic tips, mGluR6 receptors
549 clustered on these tips which came in close contact with presynaptic ribbons (Fig. 5G-5I). These
550 newly formed synaptic structures supported normal neural transmission, as shown by ERG
551 recordings and patch recordings from rod bipolar cells (Fig. 6), and light sensitivity in increased
552 in RGCs (Fig. 7). We hypothesize that these changes may be initiated by glutamate release at
553 the rod's synapse, similar to that which occurs at the cortex, where focal uncaging of glutamate
554 in mouse cortical layer 2/3 pyramidal neurons triggered spinogenesis from the dendrite shaft in
555 a location-specific manner (Kwon and Sabatini, 2011).

556 Plasticity at the photoreceptor/bipolar cell synapse has also been observed in a model of
557 photocoagulation of rabbit retina, where the laser ablation acutely removes a patch of
558 photoreceptors while leaving the inner retina intact (Beier et al., 2017). After some days, nearby
559 photoreceptors slowly migrate toward and fill in the lesioned area (Sher et al., 2013). As they do
560 so, they form functional contacts with the deafferented bipolar cells (Sher et al., 2013; Beier et
561 al., 2017). Another example of plasticity at the photoreceptor/bipolar cell synapse is the AAV-
562 mediated gene therapy to replace retinoschisin (RS1) in adult mice (Ou et al., 2015). Retinal
563 development of the RS1 knockout mice appears to proceed normally. However, the absence of
564 RS1, a cell adhesion protein, eventually causes splitting of the retina and a failure of synaptic
565 maintenance that manifests in reduction of the ERG b-wave amplitude (Sikkink et al., 2007).
566 This defect was reversed upon RS1 gene replacement (Ou et al., 2015). Here we demonstrate
567 for the first time that activation of rod input in young adults reversed synaptic changes that
568 occurred during development and established functional contacts with their downstream
569 neurons in the retinal circuitry of the adult retina. These results support the therapeutic potential
570 of repairing or replacing defective rods in the degenerating retina. However, a critical time
571 window for rescue likely exists: recent clinical trials for Leber Congenital Amaurosis to replace
572 RPE65 in human patients for treating a type of Leber's congenital amaurosis (LCA) caused by
573 RPE65 mutations show limited success in visual improvement, and the retina continued to
574 degenerate in some patients (Cideciyan et al., 2013). Future experimentation will address
575 whether a critical time window of rescue exists for these approaches.

576 **References**

577


578 Anastassov IA, Wang W, Dunn FA (2017) Synaptogenesis and synaptic protein localization in
579 the postnatal development of rod bipolar cell dendrites in mouse retina. J Comp Neurol.
580 Bareil C, Hamel CP, Delague V, Arnaud B, Demaille J, Claustres M (2001) Segregation of a
581 mutation in CNGB1 encoding the beta-subunit of the rod cGMP-gated channel in a
582 family with autosomal recessive retinitis pigmentosa. Hum Genet 108:328-334.
583 Bech-Hansen NT, Naylor MJ, Maybaum TA, Pearce WG, Koop B, Fishman GA, Mets M,
584 Musarella MA, Boycott KM (1998) Loss-of-function mutations in a calcium-channel
585 alpha1-subunit gene in Xp11.23 cause incomplete X-linked congenital stationary night
586 blindness. Nat Genet 19:264-267.
587 Beier C, Hovhannisyan A, Weiser S, Kung J, Lee S, Lee DY, Huie P, Dalal R, Palanker D, Sher
588 A (2017) Deafferented Adult Rod Bipolar Cells Create New Synapses with
589 Photoreceptors to Restore Vision. J Neurosci 37:4635-4644.
590 Bermingham-McDonogh O, Reh TA (2011) Regulated reprogramming in the regeneration of
591 sensory receptor cells. Neuron 71:389-405.
592 Biel M, Michalakis S (2007) Function and dysfunction of CNG channels: insights from
593 channelopathies and mouse models. Molecular neurobiology 35:266-277.
594 Boycott KM, Pearce WG, Bech-Hansen NT (2000) Clinical variability among patients with
595 incomplete X-linked congenital stationary night blindness and a founder mutation in
596 CACNA1F. Can J Ophthalmol 35:204-213.
597 Cao Y, Sarria I, Fehlhaber KE, Kamasawa N, Orlandi C, James KN, Hazen JL, Gardner MR,
598 Farzan M, Lee A, Baker S, Baldwin K, Sampath AP, Martemyanov KA (2015)
599 Mechanism for Selective Synaptic Wiring of Rod Photoreceptors into the Retinal
600 Circuitry and Its Role in Vision. Neuron 87:1248-1260.
601 Chang B, Hawes NL, Pardue MT, German AM, Hurd RE, Davisson MT, Nusinowitz S,
602 Rengarajan K, Boyd AP, Sidney SS, Phillips MJ, Stewart RE, Chaudhury R, Nickerson
603 JM, Heckenlively JR, Boatright JH (2007) Two mouse retinal degenerations caused by
604 missense mutations in the beta-subunit of rod cGMP phosphodiesterase gene. Vision
605 Res 47:624-633.
606 Chen J, Woodruff ML, Wang T, Concepcion FA, Tranchina D, Fain GL (2010) Channel
607 modulation and the mechanism of light adaptation in mouse rods. The Journal of
608 neuroscience : the official journal of the Society for Neuroscience 30:16232-16240.
609 Chichilnisky EJ, Rieke F (2005) Detection sensitivity and temporal resolution of visual signals
610 near absolute threshold in the salamander retina. The Journal of neuroscience : the
611 official journal of the Society for Neuroscience 25:318-330.
612 Chua J, Fletcher EL, Kalloniatis M (2009) Functional remodeling of glutamate receptors by inner
613 retinal neurons occurs from an early stage of retinal degeneration. J Comp Neurol
614 514:473-491.
615 Cideciyan AV, Jacobson SG, Beltran WA, Sumaroka A, Swider M, Iwabe S, Roman AJ,
616 Olivares MB, Schwartz SB, Komaromy AM, Hauswirth WW, Aguirre GD (2013) Human
617 retinal gene therapy for Leber congenital amaurosis shows advancing retinal
618 degeneration despite enduring visual improvement. Proceedings of the National
619 Academy of Sciences of the United States of America 110:E517-525.
620 Concepcion F, Chen J (2010) Q344ter mutation causes mislocalization of rhodopsin molecules
621 that are catalytically active: a mouse model of Q344ter-induced retinal degeneration.
622 PLoS One 5:e10904.
623 Cook NJ, Molday LL, Reid D, Kaupp UB, Molday RS (1989) The cGMP-gated channel of bovine
624 rod photoreceptors is localized exclusively in the plasma membrane. J Biol Chem
625 264:6996-6999.

626 D'Orazi FD, Suzuki SC, Wong RO (2014) Neuronal remodeling in retinal circuit assembly,
627 disassembly, and reassembly. Trends Neurosci 37:594-603.
628 Dacheux RF, Raviola E (1986) The rod pathway in the rabbit retina: a depolarizing bipolar and
629 amacrine cell. The Journal of neuroscience : the official journal of the Society for
630 Neuroscience 6:331-345.
631 Dizhoor AM, Olshevskaya EV, Peshenko IV (2010) Mg2+/Ca2+ cation binding cycle of guanylyl
632 cyclase activating proteins (GCAPs): role in regulation of photoreceptor guanylyl
633 cyclase. Mol Cell Biochem 334:117-124.
634 Farber DB, Lolley RN (1974) Cyclic guanosine monophosphate: elevation in degenerating
635 photoreceptor cells of the C3H mouse retina. Science 186:449-451.
636 Field GD, Rieke F (2002) Nonlinear signal transfer from mouse rods to bipolar cells and
637 implications for visual sensitivity. Neuron 34:773-785.
638 Field GD, Sampath AP (2017) Behavioural and physiological limits to vision in mammals. Philos
639 Trans R Soc Lond B Biol Sci 372.
640 Field GD, Gauthier JL, Sher A, Greschner M, Machado TA, Jepson LH, Shlens J, Gunning DE,
641 Mathieson K, Dabrowski W, Paninski L, Litke AM, Chichilnisky EJ (2010) Functional
642 connectivity in the retina at the resolution of photoreceptors. Nature 467:673-677.
643 Garg A, Yang J, Lee W, Tsang SH (2017) Stem Cell Therapies in Retinal Disorders. Cells 6.
644 Granit R (1933) The components of the retinal action potential in mammals and their relation to
645 the discharge in the optic nerve. J Physiol 77:207-239.
646 Grunwald ME, Yu WP, Yu HH, Yau KW (1998) Identification of a domain on the beta-subunit of
647 the rod cGMP-gated cation channel that mediates inhibition by calcium-calmodulin. J
648 Biol Chem 273:9148-9157.
649 Haeseleer F, Imanishi Y, Maeda T, Possin DE, Maeda A, Lee A, Rieke F, Palczewski K (2004)
650 Essential role of Ca2+-binding protein 4, a Cav1.4 channel regulator, in photoreceptor
651 synaptic function. Nat Neurosci 7:1079-1087.
652 Hayashi S, McMahon AP (2002) Efficient recombination in diverse tissues by a tamoxifen-
653 inducible form of Cre: a tool for temporally regulated gene activation/inactivation in the
654 mouse. Dev Biol 244:305-318.
655 Hoyo NL, Lopez-Begines S, Rosa JL, Chen J, Mendez A (2014) Functional EF-hands in
656 neuronal calcium sensor GCAP2 determine its phosphorylation state and subcellular
657 distribution in vivo, and are essential for photoreceptor cell integrity. PLoS Genet
658 10:e1004480.
659 Hüttl S, Michalakis S, Seeliger M, Luo DG, Acar N, Geiger H, Hudl K, Mader R, Haverkamp S,
660 Moser M, Pfeifer A, Gerstner A, Yau KW, Biel M (2005) Impaired channel targeting and
661 retinal degeneration in mice lacking the cyclic nucleotide-gated channel subunit CNGB1.
662 J Neurosci 25:130-138.
663 Kaupp UB, Niidome T, Tanabe T, Terada S, Bonigk W, Stuhmer W, Cook NJ, Kangawa K,
664 Matsuo H, Hirose T, et al. (1989) Primary structure and functional expression from
665 complementary DNA of the rod photoreceptor cyclic GMP-gated channel. Nature
666 342:762-766.
667 Koch S, Sothilingam V, Garcia Garrido M, Tanimoto N, Becirovic E, Koch F, Seide C, Beck SC,
668 Seeliger MW, Biel M, Muhlfriedel R, Michalakis S (2012) Gene therapy restores vision
669 and delays degeneration in the CNGB1(-/-) mouse model of retinitis pigmentosa. Hum
670 Mol Genet 21:4486-4496.
671 Kwon HB, Sabatini BL (2011) Glutamate induces de novo growth of functional spines in
672 developing cortex. Nature 474:100-104.
673 Ma H, Butler MR, Thapa A, Belcher J, Yang F, Baehr W, Biel M, Michalakis S, Ding XQ (2015)
674 cGMP/Protein Kinase G Signaling Suppresses Inositol 1,4,5-Trisphosphate Receptor
675 Phosphorylation and Promotes Endoplasmic Reticulum Stress in Photoreceptors of
676 Cyclic Nucleotide-gated Channel-deficient Mice. J Biol Chem 290:20880-20892.

677 Mansergh F, Orton NC, Vessey JP, Lalonde MR, Stell WK, Tremblay F, Barnes S, Rancourt
678 DE, Bech-Hansen NT (2005) Mutation of the calcium channel gene Cacna1f disrupts
679 calcium signaling, synaptic transmission and cellular organization in mouse retina. Hum
680 Mol Genet 14:3035-3046.
681 Marc RE, Jones BW (2003) Retinal remodeling in inherited photoreceptor degenerations. Mol
682 Neurobiol 28:139-147.
683 Marc RE, Jones BW, Watt CB, Strettoi E (2003) Neural remodeling in retinal degeneration. Prog
684 Retin Eye Res 22:607-655.
685 Maxeiner S, Luo F, Tan A, Schmitz F, Sudhof TC (2016) How to make a synaptic ribbon:
686 RIBEYE deletion abolishes ribbons in retinal synapses and disrupts neurotransmitter
687 release. Embo J 35:1098-1114.
688 Mendez A, Burns ME, Sokal I, Dizhoor AM, Baehr W, Palczewski K, Baylor DA, Chen J (2001)
689 Role of guanylate cyclase-activating proteins (GCAPs) in setting the flash sensitivity of
690 rod photoreceptors. Proc Natl Acad Sci U S A 98:9948-9953.
691 Molday RS, Moritz OL (2015) Photoreceptors at a glance. J Cell Sci 128:4039-4045.
692 Ou J, Vijayasarathy C, Ziccardi L, Chen S, Zeng Y, Marangoni D, Pope JG, Bush RA, Wu Z, Li
693 W, Sieving PA (2015) Synaptic pathology and therapeutic repair in adult retinoschisis
694 mouse by AAV-RS1 transfer. J Clin Invest 125:2891-2903.
695 Pahlberg J, Frederiksen R, Pollock GE, Miyagishima KJ, Sampath AP, Cornwall MC (2017)
696 Voltage-sensitive conductances increase the sensitivity of rod photoresponses following
697 pigment bleaching. J Physiol 595:3459-3469.
698 Poetsch A, Molday LL, Molday RS (2001) The cGMP-gated channel and related glutamic acid-
699 rich proteins interact with peripherin-2 at the rim region of rod photoreceptor disc
700 membranes. J Biol Chem 276:48009-48016.
701 Puthussery T, Taylor WR (2010) Functional changes in inner retinal neurons in animal models
702 of photoreceptor degeneration. Adv Exp Med Biol 664:525-532.
703 Quartilho A, Simkiss P, Zekite A, Xing W, Wormald R, Bunce C (2016) Leading causes of
704 certifiable visual loss in England and Wales during the year ending 31 March 2013. Eye
705 (Lond) 30:602-607.
706 Sampath AP, Rieke F (2004) Selective transmission of single photon responses by saturation at
707 the rod-to-rod bipolar synapse. Neuron 41:431-443.
708 Saszik SM, Robson JG, Frishman LJ (2002) The scotopic threshold response of the dark-
709 adapted electroretinogram of the mouse. J Physiol 543:899-916.
710 Scholl HP, Strauss RW, Singh MS, Dalkara D, Roska B, Picaud S, Sahel JA (2016) Emerging
711 therapies for inherited retinal degeneration. Sci Transl Med 8:368rv366.
712 Sher A, Jones BW, Huie P, Paulus YM, Lavinsky D, Leung LS, Nomoto H, Beier C, Marc RE,
713 Palanker D (2013) Restoration of retinal structure and function after selective
714 photocoagulation. J Neurosci 33:6800-6808.
715 Sikkink SK, Biswas S, Parry NR, Stanga PE, Trump D (2007) X-linked retinoschisis: an update.
716 J Med Genet 44:225-232.
717 Soto F, Kerschensteiner D (2015) Synaptic remodeling of neuronal circuits in early retinal
718 degeneration. Front Cell Neurosci 9:395.
719 Vinberg F, Wang T, Molday RS, Chen J, Kefalov VJ (2015) A new mouse model for stationary
720 night blindness with mutant Slc24a1 explains the pathophysiology of the associated
721 human disease. Human molecular genetics 24:5915-5929.
722 Waldner DM, Bech-Hansen NT, Stell WK (2018) Channeling Vision: CaV1.4-A Critical Link in
723 Retinal Signal Transmission. Biomed Res Int 2018:7272630.
724 Wang T, Chen J (2014) Induction of the unfolded protein response by constitutive G-protein
725 signaling in rod photoreceptor cells. J Biol Chem 289:29310-29321.
726 Wang T, Tsang SH, Chen J (2017a) Two pathways of rod photoreceptor cell death induced by
727 elevated cGMP. Hum Mol Genet 26:2299-2306.

728 Wang X, Zhao L, Zhang Y, Ma W, Gonzalez SR, Fan J, Kretschmer F, Badea TC, Qian HH,
729 Wong WT (2017b) Tamoxifen Provides Structural and Functional Rescue in Murine
730 Models of Photoreceptor Degeneration. J Neurosci 37:3294-3310.
731 Wang Y, Fehlhaber KE, Sarria I, Cao Y, Ingram NT, Guerrero-Given D, Throesch B, Baldwin K,
732 Kamasawa N, Ohtsuka T, Sampath AP, Martemyanov KA (2017c) The Auxiliary Calcium
733 Channel Subunit alpha2delta4 Is Required for Axonal Elaboration, Synaptic
734 Transmission, and Wiring of Rod Photoreceptors. Neuron 93:1359-1374 e1356.
735 Yao K, Qiu S, Wang YV, Park SJH, Mohns EJ, Mehta B, Liu X, Chang B, Zenisek D, Crair MC,
736 Demb JB, Chen B (2018) Restoration of vision after de novo genesis of rod
737 photoreceptors in mammalian retinas. Nature 560:484-488.
738 Yu WQ, Grzywacz NM, Lee EJ, Field GD (2017) Cell type-specific changes in retinal ganglion
739 cell function induced by rod death and cone reorganization in rats. J Neurophysiol
740 118:434-454.
741 Zhang Y, Molday LL, Molday RS, Sarfare SS, Woodruff ML, Fain GL, Kraft TW, Pittler SJ (2009)
742 Knockout of GARPs and the beta-subunit of the rod cGMP-gated channel disrupts disk
743 morphogenesis and rod outer segment structural integrity. J Cell Sci 122:1192-1200.
744

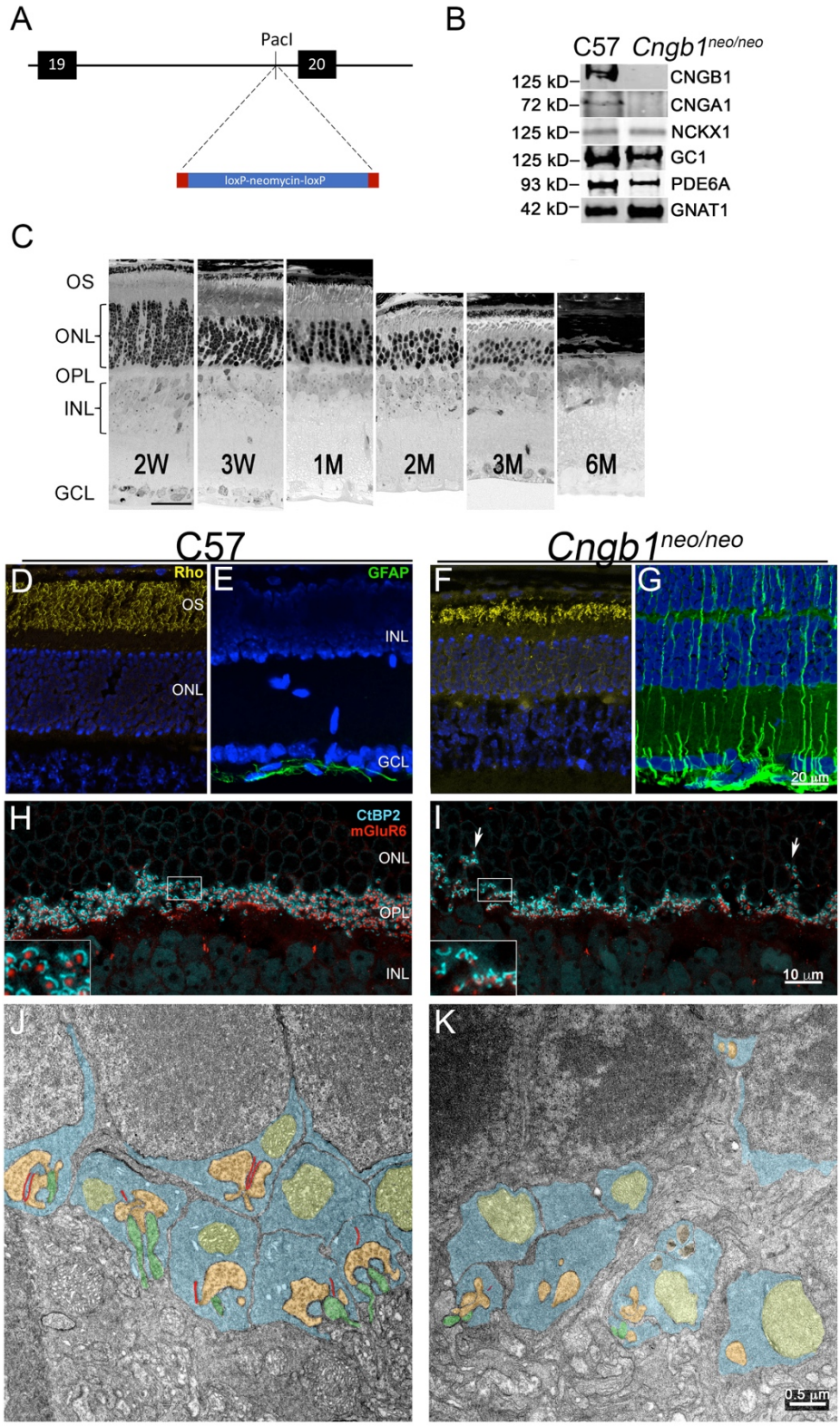
A
PacI
19
20
loxP-neomycin-loxP
B
C57
Cngb1neo/neo
125 kD–
72 kD–
125 kD–
125 kD–
93 kD–
42 kD–
CNGB1
CNGA1
NCKX1
GC1
PDE6A
GNAT1
C
OS
ONL
OPL
INL
GCL
2W
3W
1M
2M
3M
6M
C57
Cngb1neo/neo
D
Rho
OS
ONL
E
GFAP
INL
GCL
F
G
20 µm
H
CtBP2
mGluR6
ONL
OPL
INL
I
10 µm
J
K
0.5 µm

745

746 **Figure 1.** Retinas from *Cngb1*$^{neo/neo}$ mice exhibit stereotypic degenerative changes. (A) The 1.8
747 kb neomycin cassette, flanked by loxP sites, was inserted into intron 19 of the *Cngb1* gene. (B).
748 Western blots of retinal homogenates from control and *Cngb1*$^{neo/neo}$ mice show that the
749 neomycin insertion blocked expression of CNGB1, and down regulated expression of CNGA1
750 channel proteins. C. Light micrograph of representative retinal sections prepared from
751 *Cngb1*$^{neo/neo}$ mice at the indicated ages. Scale bar = 20 µm. (D-I) Cryosections from 1 MO C57
752 (left panels) and 1 MO *Cngb1*$^{neo/neo}$ mice (right panels). Rhodopsin is localized to the outer
753 segment (D) and GFAP to the inner limiting membrane proximal to the ganglion cell layer (E) in
754 C57 retina. In contrast, the outer segment of mutant retina is shortened, and rhodopsin is
755 mislocalized to the outer nuclear layer (F), and GFAP immunoreactivity extends to the entire
756 retina (G). Nuclei are stained with DAPI (blue). (H) C57 and (I) *Cngb1*$^{neo/neo}$ retinal sections
757 stained for synaptic ribbons (CtBP2, blue) of photoreceptors and mGluR6 puncta (red) of
758 bipolar cell dendrites. Transmission electron microscopy of C57 (J) and *Cngb1*$^{neo/neo}$ (K) retinal
759 sections. Color coding is as follows: rod spherule (blue), mitochondria (yellow), synaptic ribbon
760 (red), horizontal cell (orange) and rod bipolar cell (green). OS, outer segment; ONL, outer
761 nuclear layer; OPL, outer plexiform layer; INL, inner nuclear layer; GCL, ganglion cell layer.

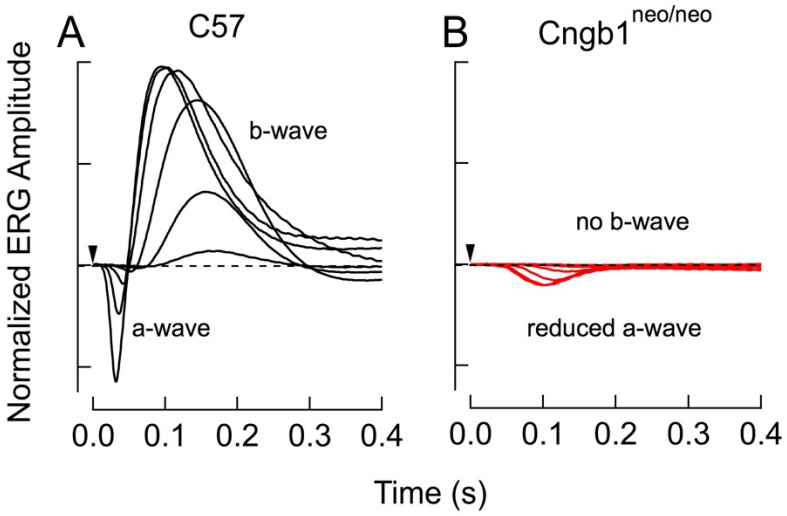


762
763
764 **Figure 2.** Characterization of rod function by *ex-vivo* electroretinography (ERGs). (A) ERG
765 recordings from a 3 MO C57 mouse show normal a- and b-waves (rod and RBC responses,
766 respectively). Flashes generated 2, 9, 35, 140, 560, and 2200 Rh*/rod (B) ERGs from 1 MO
767 *Cngb1*$^{neo/neo}$ mice show total absence of the b-wave, consistent with disrupted rod-to-RBC
768 signaling. Flashes generated 550, 2200, 8800, 18,000, and 35,000 Rh*/rod.

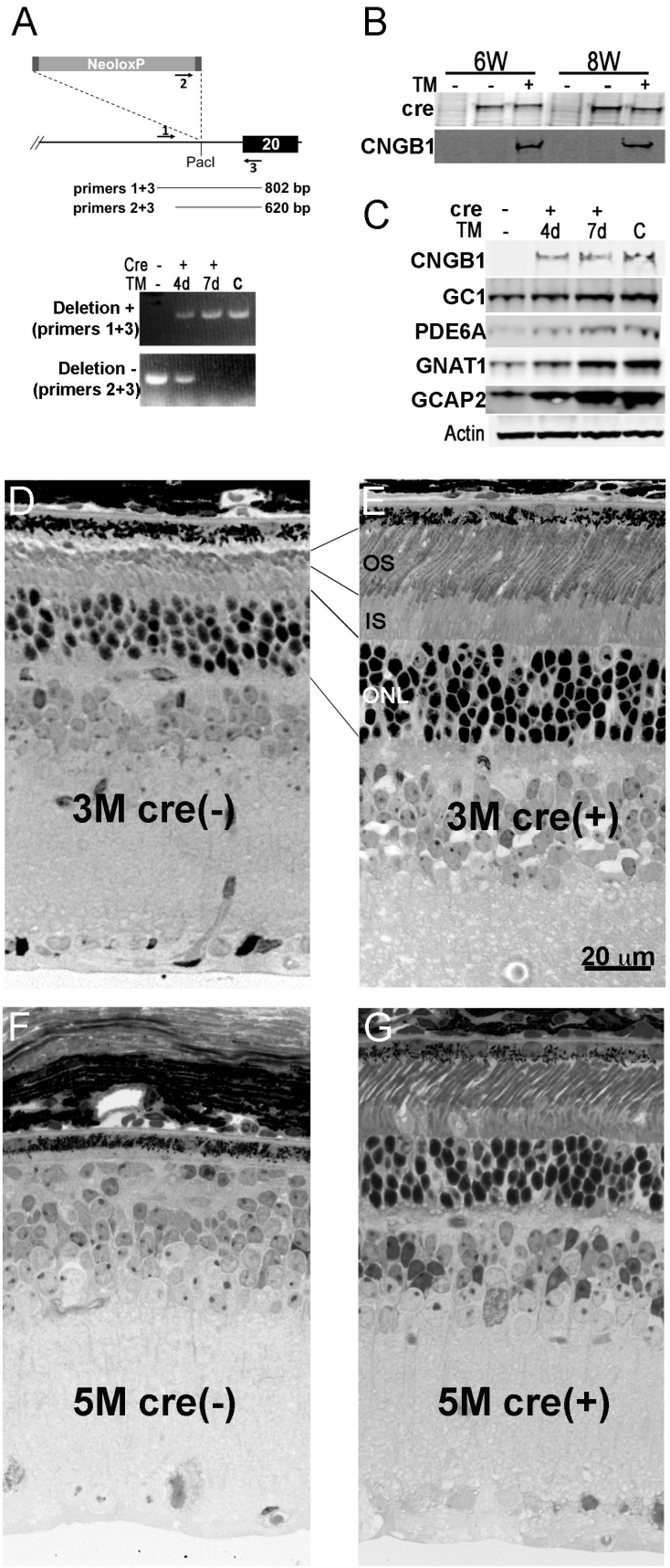
A
NeoloxP
2
1
20
PacI
3
primers 1+3
802 bp
primers 2+3
620 bp
Cre - + +
TM - 4d 7d C
Deletion +
(primers 1+3)
Deletion -
(primers 2+3)
B
6W
8W
TM - - + - - +
cre
CNGB1
C
cre - + +
TM - 4d 7d C
CNGB1
GC1
PDE6A
GNAT1
GCAP2
Actin
D
3M cre(-)
E
OS
IS
ONL
3M cre(+)
20 um
F
5M cre(-)
G
5M cre(+)

770 **Figure 3.** Excision of the floxed neomycin cassette restores CNG channel expression and
771 rescues rod cell death. (A) PCR primers 1, 2, and 3 were designed to detect the presence or
772 absence of the neoloxP cassette. Littermate mice were treated with tamoxifen (TM) for the
773 indicated number of days starting at 4 weeks and retinal DNA was extracted from mice at 8
774 weeks. Control retinal DNA "c" is from a germline-floxed mouse wherein the neoloxP cassette
775 has been removed in all tissues (*Cngb1ΔCaM*). (B) Western blots of retinal homogenates from
776 cre-negative and cre-positive littermate mice of the indicated ages (6 weeks, 8 weeks) that were
777 treated with TM or vehicle (corn oil) beginning at 4 weeks old for four consecutive days. (C)
778 Western blot of retinal homogenate prepared from the contralateral eye from mice used in (A).
779 Representative retinal morphology (N = 3) of 3 MO cre-negative (D) or cre-positive littermates
780 (E) mice treated with tamoxifen for 7 consecutive days beginning at 4 weeks. TM-treatment of
781 cre-positive mice showed improved outer segment (OS) length and thicker outer nuclear layer
782 (ONL), indicating a halt on cell death. (F) cre-negative and (G) cre-positive littermates treated
783 with tamoxifen for 4 consecutive days starting at P28, and retinal morphology was examined at
784 5 months of age (representative image from N ≥ 3). Scale bar = 20 μm.

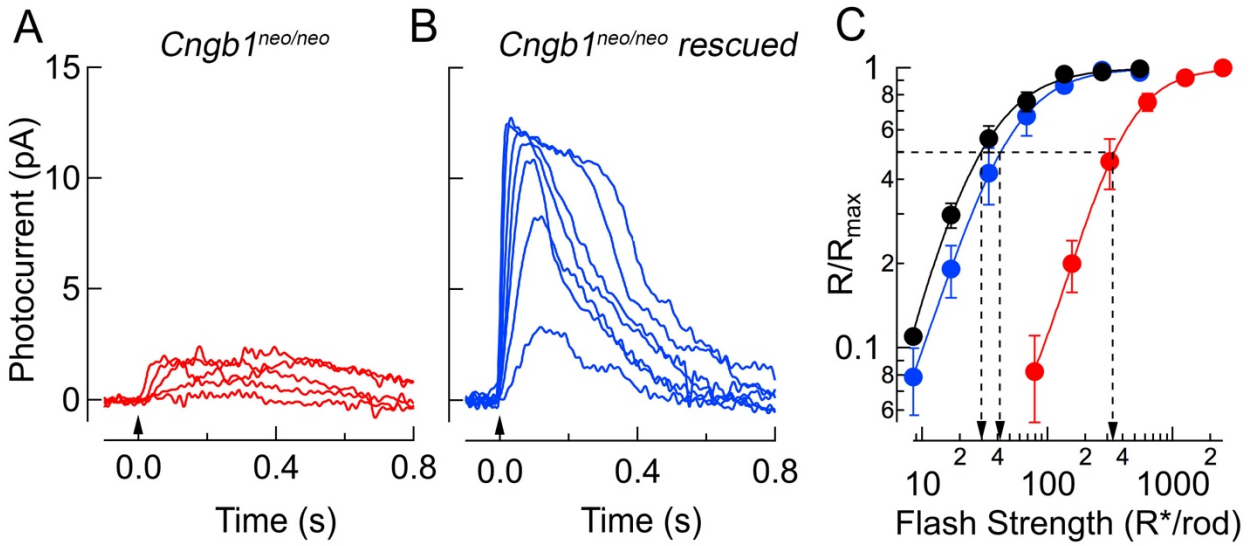


**Figure 4.** Light sensitivity is improved following expression of CNGB1. (A) Single cell recordings show small, desensitized response families in *Cngb1*$^{neo/neo}$ mice likely reflecting residual CNG channels composed of CNGA1 monomers. Flashes generated 79, 160, 310, 270, 1300, and 2500 Rh*/rod. (B) Following tamoxifen treatment, rod responses showed amplitudes and sensitivity resembling those of C57; flash strengths were 9, 17, 34, 68, 140, 270, and 540 Rh*/rod. (C) Response-intensity relationships from single-cell recordings display ~10-fold reduction in sensitivity between WT (black dots) and *Cngb1*$^{neo/neo}$ (red dots) ($I_{½}$ values were 27 ± 4 (n=5) and 360 ± 8 (n=9), respectively). This sensitivity shift is nearly restored following reintroduction of the CNGB1 (blue dots; $I_{½}$ = 43 ± 3 (n=10)).

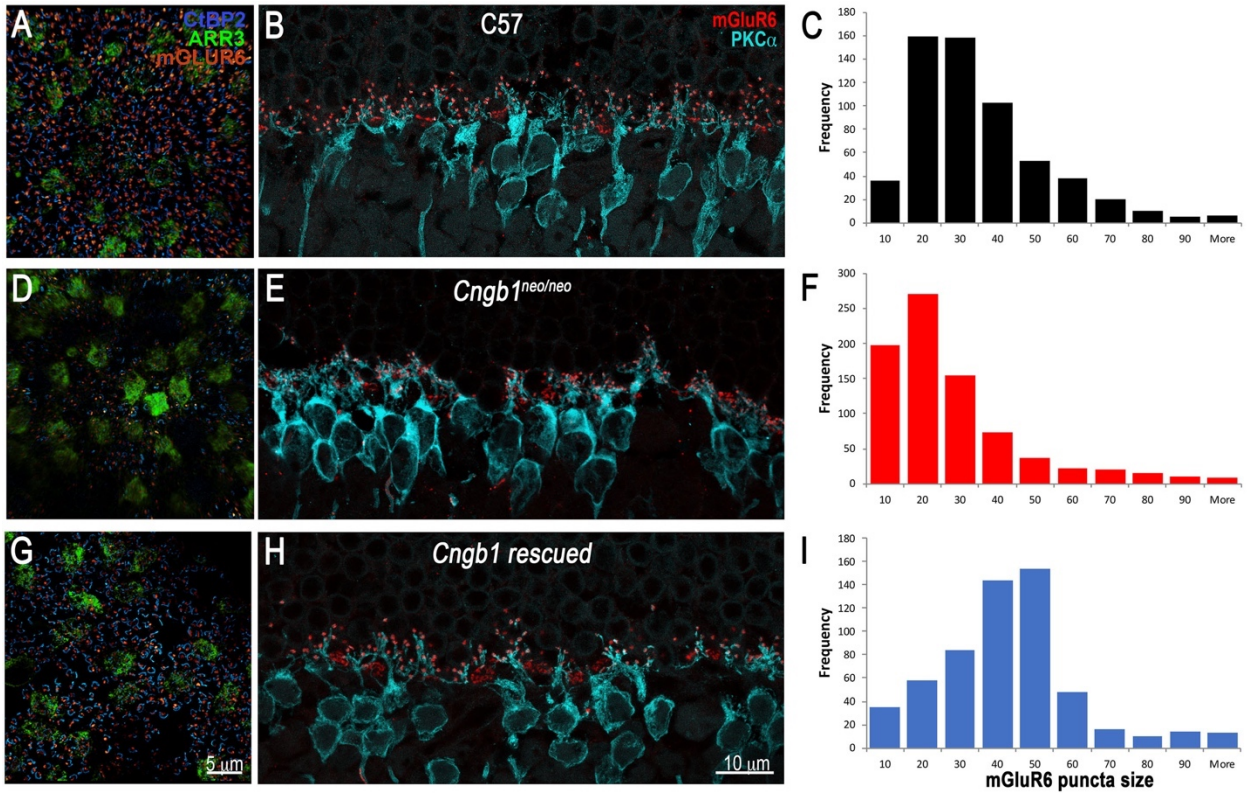


**Figure 5.** Expression of CNGB1 reverses pre- and postsynaptic retinal remodeling in *Cngb1*$^{neo/neo}$ retina. Shown are representative images from N>3 independent experiments. A, D and G are retinal flat mounts from 1 MO C57, 1 MO *Cngb1*$^{neo/neo}$ and 3 MO rescued *Cngb1* mice treated with tamoxifen for 7 consecutive days beginning at 4 weeks of age, respectively. The flat mounts were stained with the pre-synaptic ribbon marker, CtBP2 (blue), and post-synaptic marker mGluR6 (orange). Cone pedicles were visualized using cone arrestin, ARR3 (green). B, E and H are retinal cross sections from mice of the same genotype as the flat mounts. The retinal sections were stained with antibodies to mGluR6 (red) and the rod bipolar cell marker, PKCα (teal). C, F and I are frequency vs. mGluR6 puncta size distributions for 1 MO C57, 1 MO *Cngb1*$^{neo/neo}$ and 3 MO rescued *Cngb1* mice treated with tamoxifen.

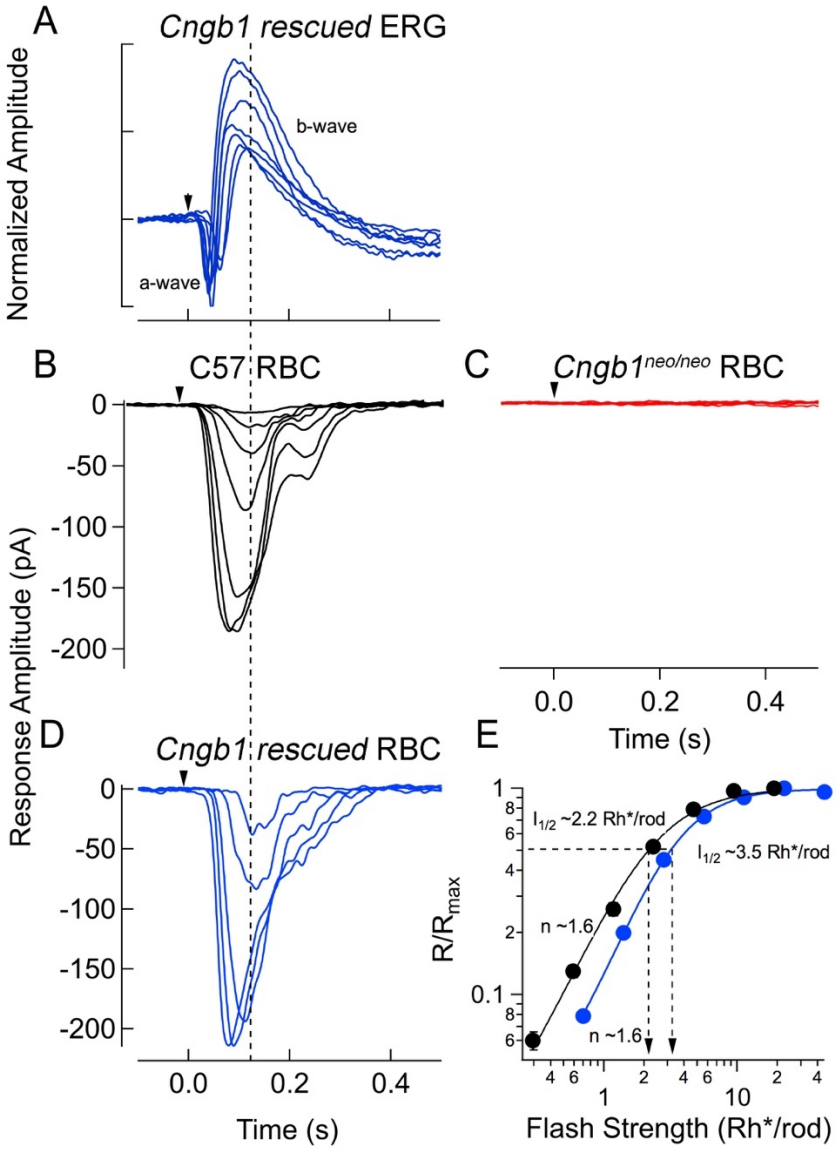


**Figure 6.** Physiological responses from rod bipolar cells in retinal slices. A. *Ex-vivo* ERG responses from 3 to 6 MO mice after tamoxifen treatments show near normal a- and b-waves. Flashes generated 2, 9, 35, 140, 550, and 2200 Rh*/rod. Please compare against Fig. 2A. Voltage-clamp rod bipolar cell recordings ($V_m$ = -60 mV) from the following mice: B. C57 rod bipolar cells (2-3 MO); C. *Cngb1*$^{neo/neo}$ rod bipolar cells (1 MO); D. *Cngb1* tamoxifen-treated (3 MO). Flashes generated 2, 4, 8, 16, 31, 62 and 130 Rh*/rod for C57 rod bipolar cells, and 280, 560, 1100 and 2200 Rh*/rod for *Cngb1*$^{neo/neo}$ rod bipolar cells. Light-evoked responses were never observed in *Cngb1*$^{neo/neo}$ rod bipolar cells (15 cells across 5 retinas – flashes generated 2200 Rh*/rod). E.Response-intensity relationships from mean data show that this relationship is shifted to higher flash strengths in rescued mice, reflecting some rod loss. The Hill exponent of rod bipolar cells were similar to normal following rod recovery (Hill exponent = 1.6 ± 0.05 (n=12)), in support of a restoration of the normal rod-to-rod bipolar cell synaptic structure and the dark rate of glutamate release.

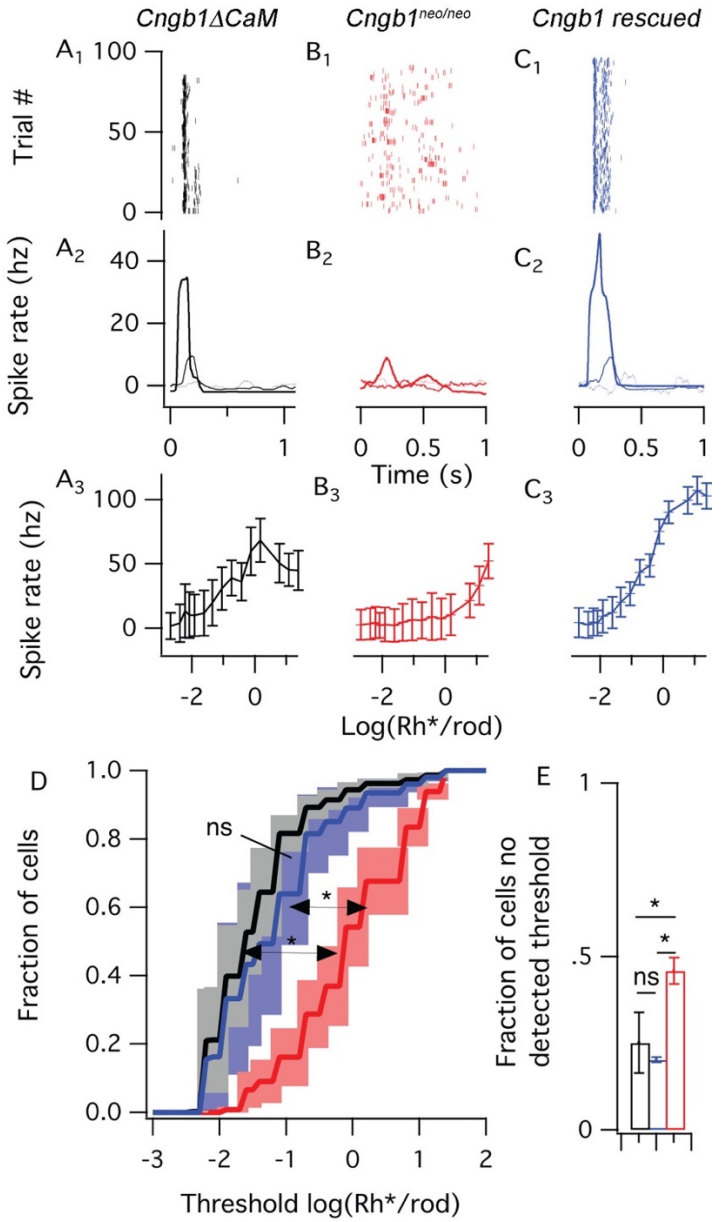


**Figure 7.** Dim flash responses from retinal ganglion cells (RGCs) in whole mount retina show recovery from early rod rescue. The top panels (A-$C_1$) show spike times of 100 trials of 3 example cells to a single dim flash (0.75 Rh*/rod). The middle panels (A-$C_2$) shows PSTHs for three increasingly bright dim flashes (0.002, 0.02, 0.75, Rh*/rod). The bottom panels (A-$C_3$) show the mean spike rate ± SD, measured on each trial in a 100 ms window around the peak of the PSTH. Dim flash thresholds were estimated from these curves for 1954 cells. The average cumulative distribution function show higher thresholds responses in *Cngb1*$^{neo/neo}$ mice RGCs than *Cngb1ΔCaM* and tamoxifen-treated *Cngb1*$^{neo/neo}$ mice RGCs (D). The shaded regions illustrating SEMs across (3-5 experimental preparations). Additionally, flash thresholds could not be identified in a larger portion of RGCs from *Cngb1*$^{neo/neo}$ mice (E).